

2015 SNMMI Highlights Lecture: Oncology, Part I

Umar Mahmood, MD, PhD, Massachusetts General Hospital, Boston, MA

From the Newsline Editor: The Highlights Lecture, presented at the closing session of each SNMMI Annual Meeting, was originated and delivered for more than 30 years by Henry N. Wagner, Jr., MD. Beginning in 2010, the duties of summarizing selected significant presentations at the meeting were divided annually among 4 distinguished nuclear and molecular medicine subject matter experts. The 2015 Highlights Lectures were delivered on June 10 at the SNMMI Annual Meeting in Baltimore, MD. Umar Mahmood, MD, PhD, a professor of radiology at Massachusetts General Hospital (Boston, MA), spoke on oncology highlights from the meeting's sessions. Because of its length, the oncology presentation will be divided between 2 Newsline issues. Note that in the following summary, numerals in brackets represent abstract numbers as published in The Journal of Nuclear Medicine [2015;56:suppl 3].

This year's SNMMI Annual Meeting featured many extraordinary presentations focusing on oncology. These included 261 basic science and 359 clinical oncology abstracts, for a total of more than 600 oncology abstracts, with far too many significant findings to be highlighted in the limited time allotted for this lecture. One interesting theme that emerged was that of "convergent evolution": many different groups are working on the same targets in different and quite creative ways. I want to emphasize that although I have selected specific approaches as examples, the methods identified in this lecture are not the only ways to image specific processes or treat individual diseases. We have a growing and diverse number of ways to image targets and cancer pathways—many will turn out to be complementary and deserve our attention and additional exploration. I also want to thank all of the investigators who sent slides of their work as I prepared this lecture. I apologize that time constraints prevent showing and discussing all of these excellent studies.

One of the highlights for me at this meeting was the Peter Valk Memorial Lecture presented on June 9 by Sanjiv Sam Gambhir, MD, PhD, the Virginia and D.K. Ludwig Professor for Clinical Investigation in Cancer Research and chair of the Department of Radiology at Stanford University School of Medicine (CA). Gambhir gave a moving and comprehensive overview of "Integrating in vitro diagnostics and molecular imaging for optimizing cancer management." As technology moves forward, we need to enhance our ability to integrate the growing amount of genomic and proteomic data coming from blood samples and other sources into our interpretation of imaging data. The science of cancer continues to accelerate in terms of understanding mechanisms of disease, cancer pathways, and cell types—and imaging science is keeping pace in new and sometimes astonishing

ways. We saw at this meeting a strong push for human translation of these innovations, with many first-in-human studies for cancer detection, for visualizing specific cancer targets, and for utilizing overexpressed cancer targets for radiotherapy. We are also seeing a real renaissance in studies on theranostics, not only with β particles but with α particles as well.



Umar Mahmood, MD, PhD

Complementary Cell-Based Assays

Yoshii et al. from the National Institute of Radiological Sciences (Chiba, Japan), SCIVAX Life Sciences, Inc. (Kawasaki, Japan), and the University of Fukui (Eiheiji, Japan) reported on "Development of drug screening system with nanoimprinting 3D culture to provide effective drugs in vivo and the accompanying PET probes for therapy monitoring" [1203]. One of the challenges in drug studies that screen cells is that these analyses are typically performed with cells in 2-dimensional (2D) monolayers, whereas cells themselves are 3D. If we think about a tumor in vivo, for example, it is a 3D matrix, with cells maintaining connections in all directions, and could be expected to react differently from cells within a typical experimental system with cell-cell contact in a single plane. These researchers developed an easy-to-use, matrix-free nanoimprinted scaffolding for 3D spheroids to facilitate testing both drugs and PET agents. With this scaffolding, in vitro studies more closely mimic in vivo studies. They found that nanoimprinting 3D screening more efficiently selected drugs that effectively inhibited cancer growth in vivo than did conventional 2D culture. They also used this approach to screen PET probes (including ^{11}C -methionine, ^{11}C -acetate, ^{18}F -fluorothymidine, and methyl- ^{11}C -thiothymidine, with comparisons to ^{18}F -FDG) for therapy monitoring. In vitro 3D spheroid uptake correlated closely with in vivo tumor uptake (Fig. 1). This technology may allow us to more rapidly screen drugs, a very real advantage as research increasingly involves placing individual patients' tumors into mice and into cell culture studies. This may allow us not only to rapidly screen for drug selection but also advance our ability to personalize use of imaging agents for optimized treatment monitoring.

In Vivo Targeted Imaging

Pyo et al. from Chonnam National University Hwasun Hospital (Republic of Korea) reported on "Synthesis and evaluation of ^{64}Cu labeled repebody for epidermal growth factor receptor (EGFR)-mediated cancer imaging in small animals" [172]. The investigators used repebodies, a new

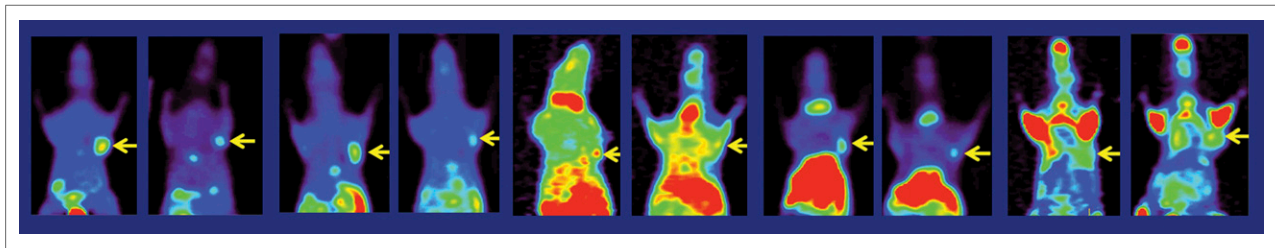


FIGURE 1. 3D nanoimprinting for PET probe selection in therapy monitoring. Validation results in 5 pairs of treatment-naïve mice and mice treated with an experimental drug, imaged with (left to right) ^{18}F -fluorothymidine (untreated left, treated right), methyl- ^{11}C -thiothymidine (untreated left, treated right), ^{11}C -acetate (untreated left, treated right), ^{11}C -methionine (untreated left, treated right), and ^{18}F -FDG (untreated left, treated right), show the high correlation between in vitro 3D model results and in vivo assessment.

type of scaffold made of nonimmunoglobulin antibodies, in this case targeted to EGFR, which is overexpressed in many cancers. Repebodies come from jawless vertebrates and, at 28 kDa, are much smaller than typical antibodies used in

such studies, a characteristic that may improve pharmacokinetics. They are called repebodies because they include leucine-rich repeat motifs. The researchers found a high, subnanomolar binding affinity for EGFR and stability across a broad pH range for the repebodies. Three different ^{64}Cu -labeled chelators were used with this repebody: ^{64}Cu -NOTA, ^{64}Cu -DOTA, and ^{64}Cu -DTPA (Fig. 2). In all 3 cases, the tracers yielded good tumor binding and tumor-to-background ratios. This scaffold could be applied to a number of different targeted imaging agents.

Kotagiri et al. from the Washington University School of Medicine (St. Louis, MO) reported on “Depth-independent phototherapy using Cerenkov radiation and titanium dioxide nanoparticles” [643]. The researchers used ^{18}F -FDG with titanium dioxide nanoparticles, so that the Cerenkov radiation from the ^{18}F -FDG resulted in free radical formation at the surface of the nanoparticles, with the potential for increased cell killing capabilities. When a ~ 1 mCi dose of ^{18}F -FDG or

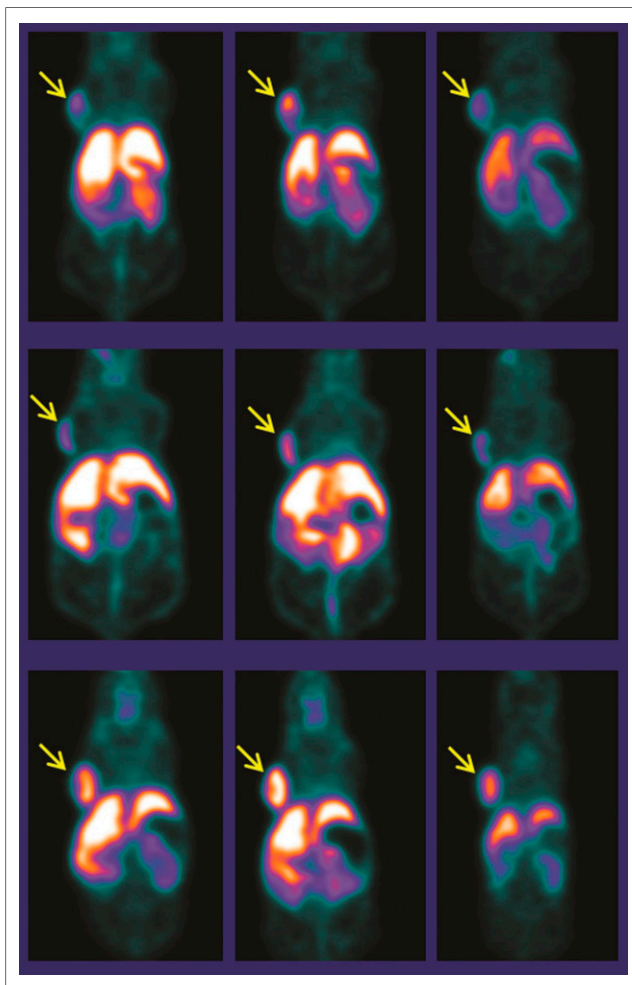


FIGURE 2. Small animal PET imaging of uptake of ^{64}Cu -NOTA-repebody, ^{64}Cu -DOTA-repebody, and ^{64}Cu -DTPA-repebody in grafted H1650 models at 1 (left), 6 (middle), and 24 (right) h after injection.

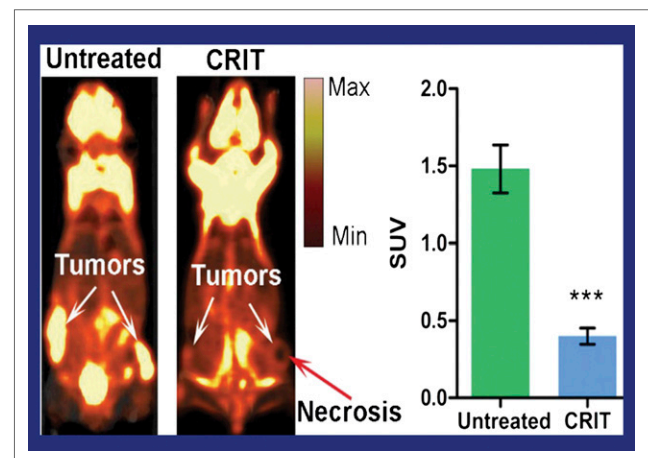


FIGURE 3. Depth-independent phototherapy with Cerenkov radiation and titanium dioxide nanoparticles. Left block: Untreated mouse (left) with bilateral HT1080 tumors (arrows) and decreased tracer uptake after treatment (right) with both ^{18}F -FDG and titanium dioxide nanoparticles demonstrates response. Note the necrotic zone in the right tumor (red arrow). Right block: ^{18}F -FDG uptake in untreated controls (green) and after combination therapy (blue) as quantified by SUV.

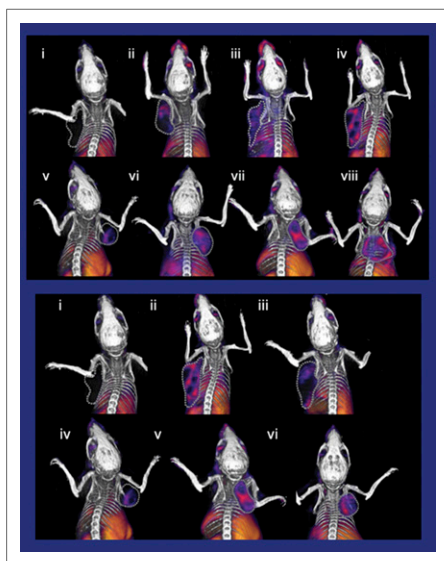


FIGURE 4. Imaging PARP-1 activity after therapeutic interventions. Top block: Dose and time dependence of ^{18}F -SuPAR uptake after radiation therapy in mice bearing MDA-MB-231 breast (top row) and HeLa cervical (bottom row) tumors (left to right) untreated, at 8 h after 5-Gy therapy, at 8 h after 10-Gy therapy, and at 24 h after 10-Gy therapy.

Both tumors showed radiation dose-dependent increases in tracer uptake, but HeLa uptake peaked 8 h after radiation, whereas uptake in MDA-MB-231 continued to increase at 24 h. Bottom block: Monitoring PARP-1 inhibition (talazoparib) with ^{18}F -SuPAR imaging in MDA-MB-231 (top row) and HeLa (bottom row) mice (left to right) untreated, after radiation, and after radiation plus talazoparib. PARP-1 inhibition significantly reduced tracer uptake only in MDA-MB-231 and not HeLa cells, suggesting the proposed use of this drug for breast cancer therapy.

titanium nanoparticles were administered separately to HT1080 tumors in a mouse model, no improved survival was noted. When these were combined, however, improvement was evident in both survival and delay in tumor growth (Fig. 3). This mechanism, converting the Cerenkov radiation into free radicals, is an interesting and promising combination of PET and optical-based therapy.

Shuhendler et al. from Stanford University (CA) and the Jiangsu Institute of Nuclear Medicine (Wuxi, China) reported on “Imaging poly(ADP ribose) polymerase-1 activity for personalized cancer medicine using a novel PET tracer” [2]. Poly(ADP ribose) polymerase-1 or PARP-1 is used by cells to repair single-strand DNA breaks. This group used PARP-1 activity as a way of imaging radiation damage. Uptake of the PET agent they developed, ^{18}F -SuPAR, increased after 15 Gy of radiation. They performed kinetic modeling and showed a significant increase in binding potential with radiation treatment and a significant decrease with PARP-1 inhibitors. They also showed, using *in vivo* click chemistry, that this uptake was specific for PARP expression. They translated these studies in mouse models, and identified a dose and time dependence of the ^{18}F -SuPAR PET agent following radiotherapy at 5 and 10 Gy and at 8 and 24 h, showing that the cell lines have different responses (Fig. 4). They also showed that PARP inhibition changes response, depending on the cell line. This work indicates the potential for enhancing timing and dosing of PARP inhibitors, or optimizing timing of other additional therapy, combined with radiation therapy.

Nicolas et al. from University Hospital Basel (Switzerland), Octeopharm Sciences GmbH (Berlin, Germany), and University Hospital Freiburg (Germany) reported on “Wider safety window with radiolabeled somatostatin receptor (SSTR) antagonists over agonists” [335]. The results of this work suggested that antagonists may be better than agonists for SSTR imaging and therapy, with a wider safety window. Gallium-based SSTR imaging is often used for diagnosis, coupled with subsequent lutetium- or yttrium-based SSTR-targeted therapies. In this case, the researchers compared the pharmacokinetics of the antagonist ^{177}Lu -OPS201 with the agonist ^{177}Lu -DOTA-TATE in HEK-hsst2 xenografts in mice and found 35% higher tumor uptake with ^{177}Lu -OPS201, with 2.5 fold longer tumor residence time, but 1.8-fold higher kidney dose, resulting in a 2.5-fold higher tumor dose and 34% improvement in tumor-to-kidney dose ratio. NanoSPECT/CT imaging at 4 h after injection showed that rather than blocking uptake, increased peptide mass improved image contrast and therapeutic index. Progression from 20 to 2,000 pmolar of ^{177}Lu -OPS201 resulted in increased uptake in these tumors, whereas liver uptake decreased (Fig. 5), indicating that the SSTR antagonist will behave somewhat differently from the agonist in imaging this target.

As noted previously, theranostics was the focus of much attention at this meeting. Heskamp et al. from Radboud University Medical Center (Nijmegen, The Netherlands), University of Wisconsin (Madison), University of Bonn (Germany), Institute for Transuranium Elements (Karlsruhe, Germany), and Universitat München (Germany) reported on “Pretargeted radioimmunotherapy with ^{213}Bi in mice with carcinoembryonic antigen (CEA)-expressing colon cancer xenografts” [9]. The investigators used a bispecific antibody targeting both CEA, resulting in tumor binding as well as targeting of histamine-succinyl-glycine (HSG) as the other

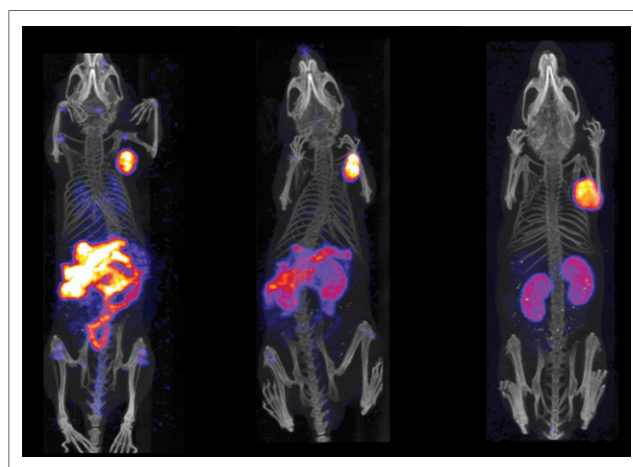


FIGURE 5. NanoSPECT/CT imaging at 4 h after injection of (left to right) 20, 200, and 2,000 pmol of ^{177}Lu -OPS201 in mice with HEK-hsst2 xenografts, indicating that increased peptide mass improves image contrast and therapeutic index.

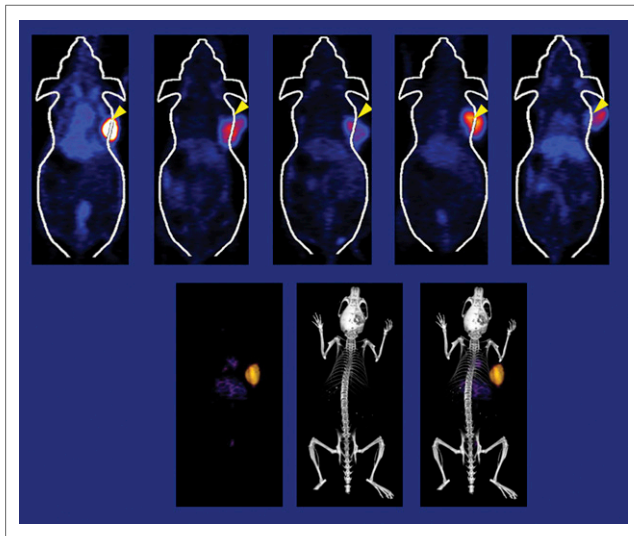


FIGURE 6. Bs-F(ab)₂-enhanced tumor-specific targeting in athymic nude mice bearing U87MG tumors, with endothelial cells positive for CD105, and tumor cells positive for EGFR. Top: PET imaging at 36 h: (left to right) ⁶⁴Cu-NOTA-Bs-F(ab)₂, ⁶⁴Cu-NOTA-CET-Fab, ⁶⁴Cu-NOTA-TRC105-Fab, ⁶⁴Cu-NOTA-Bs-F(ab)₂ plus CET blocking, and ⁶⁴Cu-NOTA-Bs-F(ab)₂ plus TRC105 blocking. Bottom: PET/CT of ⁶⁴Cu-NOTA-Bs-F(ab)₂: (left to right) PET, CT, and PET/CT, demonstrating that the 2 targeting moieties synergistically increase tumor uptake.

binding site. One day after administering this bispecific antibody, the researchers administered a di-HSG-DOTA peptide (IMP288), labeled with either ²¹³Bi or ¹⁷⁷Lu for therapy. Because the antibody did not internalize, it was still present on the surface, so the therapeutic peptide could reach it quite quickly. They found that administration of the ²¹³Bi-IMP288 resulted in tumor growth delay comparable to that with ¹⁷⁷Lu-IMP288. The authors concluded that ²¹³Bi-IMP288, when combined with the bispecific antibody, specifically targeted CEA-expressing xenografts and significantly inhibited growth of these xenografts, prolonging survival in mice. They added that ²¹³Bi-IMP288 appears to be at least as therapeutically effective as ¹⁷⁷Lu-IMP288. In some cases, depending on the desired radius of cell killing from the target location, α emitters may be preferable to β emitters.

Another interesting imaging agent came from Luo et al. from the University of Wisconsin (Madison), who reported on “Synergistically enhanced tumor uptake via dual targeting of CD105 and EGFR using a ‘click’ heterodimer” [1]. They combined 2 different targeting moieties, CD105, targeting new endothelial cells in tumors making blood vessels, and EGFR, overexpressed in a number of tumors. They combined these 2 to create a heterodimer, Bs-F(ab)₂, with 1 F(ab) fragment that targets the CD105 and another that targets the EGFR. In U87MG mice the ⁶⁴Cu-labeled NOTA-Bs-F(ab)₂ was found to have higher target uptake compared with either of the ⁶⁴Cu-labeled moieties alone. Blocking studies led to significantly reduced uptake, indicating that the very high tumor uptake with the heterodimer was the result of dual targeting of EGFR and CD105 in the tumor (Fig. 6). Low liver/kidney uptake was also observed with the heterodimer, providing excellent tumor-to-normal tissue ratios. This synergistic effect was confirmed in additional immunohistochemistry studies. This approach, using 2 different targets, one expressed on the vessels and one expressed on the tumor cells, is both interesting and promising.

Immunotherapy is the focus of much interest and seems to be in the news with increasing frequency. Several different approaches are being used, and although I will highlight 2 ways to image immune responsiveness, there are a number of other ways to approach this. Heskamp et al. from the Radboud University Medical Center (Nijmegen, The Netherlands) and INSERM Centre de Recherche en Cancérologie de Marseille (France) reported on “SPECT/CT imaging of tumor PD-L1 expression using radiolabeled anti-PD-L1 antibodies” [116]. The investigators labeled their anti-PD-L1 agent with ¹¹¹In and, in in vitro cellular uptake studies, showed that it had increased specific accumulation in several breast cancer cells overexpressing the target. SPECT/CT was acquired in 5 xenograft models with different PD-L1 expression levels (Fig. 7), with results that correlated well with in vitro studies. This demonstration of the feasibility of noninvasive imaging of PD-L1 expression in tumors may help to identify which tumors will respond to specific immunotherapies and can potentially be used to monitor tumor PD-L1 expression over the course of treatment and disease progression.

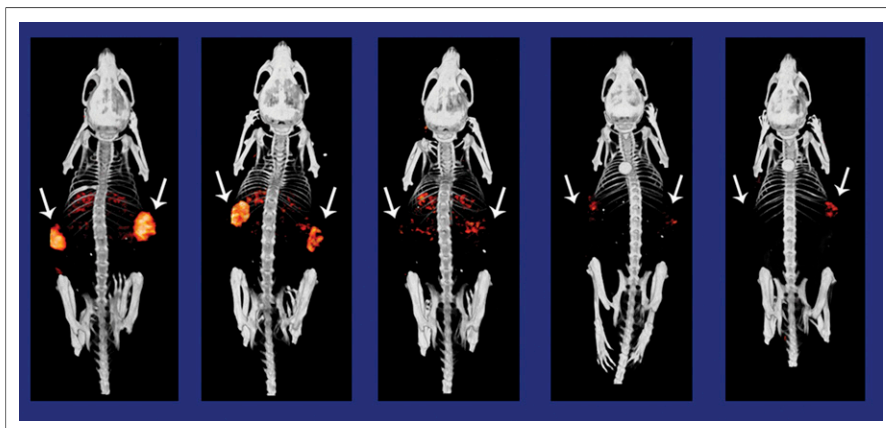


FIGURE 7. ¹¹¹In-PD-L1 SPECT/CT of different PD-L1 expression levels in 5 xenograft models: (left to right) MDA-MB-231, SK-Br-3, SUM149, BT474, and MCF-7.

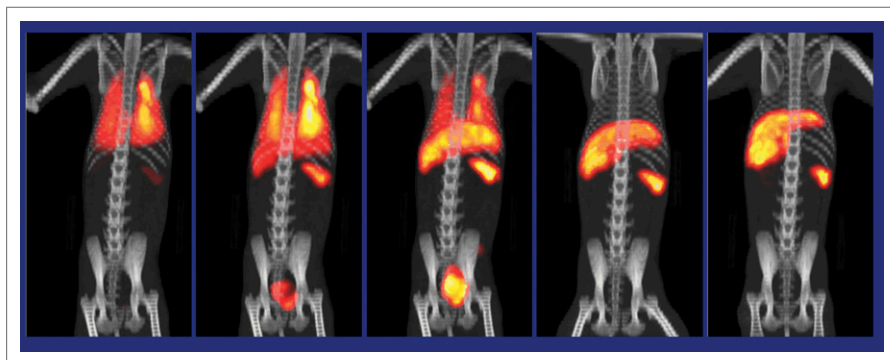


FIGURE 8. PET/CT imaging of ^{89}Zr -oxine-labeled natural killer (NK) cells autologously transferred in rhesus macaques at (left to right) 15 min, 1 h, 4 h, 2 d, and 7 d. Imaging showed that NK cells initially localized to the lungs and gradually trafficked to the liver and spleen, where they remained up to d 7.

Any number of approaches can be used in assessing immunotherapy, from directly imaging the tumor cells that may be responsive, to imaging different immune cell types that might infiltrate a tumor. Sato et al. from the National Cancer Institute (Bethesda and Frederick, MD), the National Heart, Lung, and Blood Institute (Bethesda, MD), and the National Institutes of Health Clinical Center (Bethesda, MD) reported on “Tracking adoptively transferred natural killer (NK) cells in rhesus macaques with ^{89}Zr PET imaging” [225]. NK cells are cytotoxic lymphocytes. These researchers generated an ^{89}Zr -oxine complex cell-labeling agent, evaluated the complex in vitro in rhesus macaque and human NK cells, and monitored an autologous NK cell transfer in the nonhuman primates (NHPs) with PET/CT. They found that the ^{89}Zr -oxine complex stably labeled the cells and altered neither cellular phenotype nor cytotoxic function in either NHP or human NK cells. PET/CT imaging of transferred NK cells showed trafficking of the cells to the liver and spleen, passing through the lungs. Given the long half-life of zirconium, they were able to trace these cells out over a number of days (Fig. 8). This ^{89}Zr -oxine complex thus enabled NK cell tracking at low radioactivity doses in this NHP model on a clinical PET/CT scanner.

Cancer therapy is sometimes a little bit like playing whack-a-mole. Everything is connected; as one pathway is shut down, another may compensate. Antunes et al. from University Medical Center Groningen (The Netherlands) reported on “Monitoring the crosstalk between estrogen receptor (ER) and HER2 with PET” [506]. These 2 pathways are often overexpressed in breast cancer. With ^{18}F -fluoroestradiol (^{18}F -FES) PET imaging they showed that as they used trastuzumab, which blocks HER2, in the treatment of SKOV3 xenografts that FES uptake increased, suggesting that ER expression increased to partially compensate for HER2 blocking (Fig. 9A). In assessing therapeutic strategies in cancer, sometimes imaging approaches like this may help identify which additional drugs to give to double-down to block a pathway or to shut down compensatory pathways. When researchers treated the SKOV3 xenografts with fulvestrant to decrease ER signaling and availability, using an ^{89}Zr -trastuzumab PET imaging agent, they showed that HER2 expression increased to compensate for this block (Fig. 9B). These results confirmed crosstalk between ER and HER2, demonstrated the feasibility of PET for assessing this crosstalk, and implied

that in these and other cancer pathways more than 1 drug may be required to shut both down.

Evans et al. from the University of California, San Francisco and Memorial Sloan–Kettering Cancer Center (New York, NY) developed 3 different ^{89}Zr -labeled antibodies and reported on these in “Imaging androgen receptor signaling in prostate cancer with PET” [175]. We know about prostate-specific membrane antigen (PMSA) and prostate-specific antigen (PSA) imaging. This group also developed an antibody to 6-transmembrane epithelial antigen of the prostate–1 (STEAP-1), which is downstream from androgen receptor signaling. It is currently unclear whether androgen receptors up- or downregulate STEAP-1, with implications for how the radiotracer and a companion antibody/drug conjugate should be used in castrate-resistant prostate cancer. In preclinical studies, relative declines in STEAP-1 expression triggered by inhibiting androgen receptors with orchiectomy were quantified with ^{89}Zr -2109A and used as the basis for future clinical study planning. If STEAP-1 is androgen repressed, then upregulation after antiandrogen therapy argues for combination with enzalutamide or abiraterone

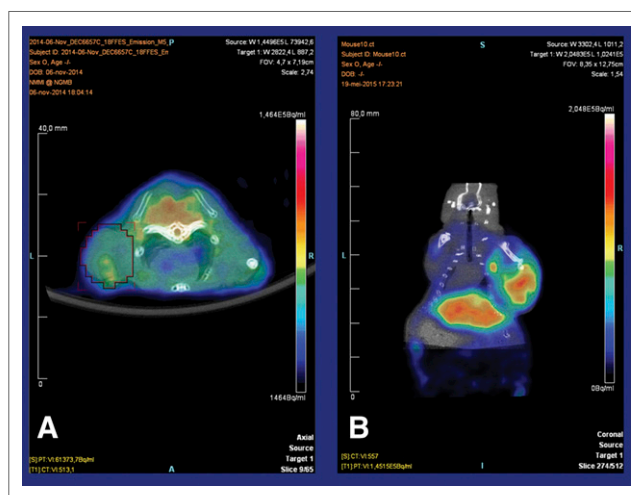


FIGURE 9. (A) ^{18}F -FES PET imaging. Treatment of SKOV3 xenografts with trastuzumab, which binds HER2, increased estrogen receptor expression. (B) ^{89}Zr -trastuzumab PET imaging. Treatment of SKOV3 xenografts with fulvestrant, which decreases free estrogen receptor, increased HER2 expression.

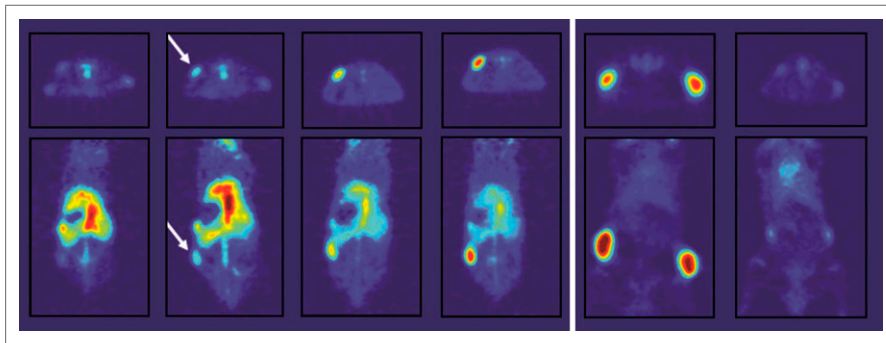


FIGURE 10. ^{89}Zr -2109A (STEAP1) PET imaging of androgen receptor signaling in prostate cancer xenografts. Left block: Increasing uptake in tumors (arrows) at (left to right) 1, 8, 24, and 48 h. Right block: Tumor uptake in vivo is inhibited by orchiectomy (right) compared with no treatment (left).

to improve the duration of response. If STEAP-1 is down-regulated, it could be used to measure the extent of androgen inhibition. Preclinical ^{89}Zr -2109A PET showed the STEAP-1 uptake in xenografts, which accumulated over the course of several days; with orchiectomy this uptake significantly decreased (Fig. 10). Clinical imaging with this tracer has the potential to provide valuable information for individualized regimens or dosing combinations in androgen receptor therapy in castrate-resistant prostate cancer.

Clinical translation

The field of radiogenomics uses imaging to help to identify genetic changes in tumors. Guillén Valderrama et al. from the Clínica Universidad de Navarra (Pamplona, Spain) and the Complejo Hospitalario de Navarra (Pamplona, Spain) reported on “Contribution of FDG PET/CT for the prediction of EGFR, KRAS mutation, and ALK rearrangement in patients with non-small cell lung cancer (NSCLC)” [642]. The study included 162 NSCLC patients (98 men, 64 women) who underwent initial ^{18}F -FDG PET/CT staging for NSCLC using standard parameters and assessing tumor, lymph nodes, and distant metastases (Fig. 11). The researchers found that patients with ALK and KRAS mutations had higher uptake in tumor lesions and nodal metastases than patients with EGFR or wild-type mutations. This type of finding is not useful on an individual basis, but potentially

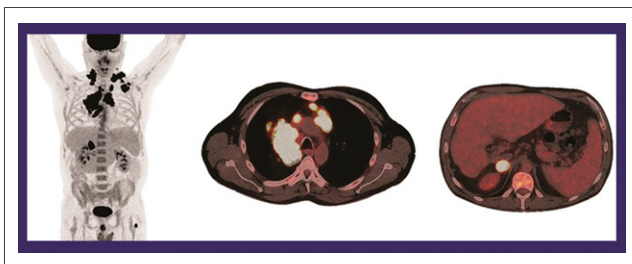


FIGURE 11. Patients with ALK and KRAS mutations presented higher ^{18}F -FDG uptake for tumor lesions and nodal metastases than those with epidermal growth factor receptor-expressing or wild-type tumors. Example images in patient with adenocarcinoma and ALK mutation. Left: maximum-intensity projection; middle: tumor and lymph nodes; right: distant metastases.

can be used in multivariate analyses to increase cohorts that are likely to have some of these mutations.

A large multicenter randomized treatment-intensification trial for high-risk non-Hodgkin lymphoma (NHL) patients stratified by ^{18}F -FDG PET was reported on at the meeting. Müller et al. from the Universitätsklinikum Essen (Germany) and Medizinische Hochschule Hannover (Germany) reported on “Positron emission tomography guided therapy of aggressive lymphoma (PETAL)—the predictive value of quantitative PET” [210]. The study included 851 intent-to-treat patients who underwent interim PET imaging after 2 cycles of combined rituximab, cyclophosphamide, doxorubicin hydrochloride, vincristine sulfate, and prednisone (R-CHOP) chemotherapy. Patients were classified as responders or non-responders based on PET findings (using a cutoff of change in standardized uptake value (SUV) $>66\%$ or $\leq 66\%$, respectively). Patients who responded progressed to standard therapy; those who did not were switched to intensive therapy in an effort to increase overall survival and time to treatment failure. Although no significant differences in overall survival or time to failure were found in outcomes for those

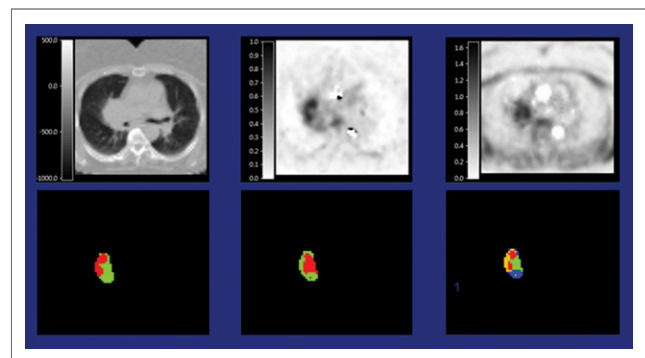


FIGURE 12. Multiparametric evaluation of tumor hypoxia and perfusion using ^{18}F -FAZA and ^{15}O - H_2O PET in a patient with non-small cell lung cancer. Top, left to right: CT, with tumor localized in the right lung; parametric image of K_1 , ^{15}O - H_2O (perfusion); and volume distribution of ^{18}F -FAZA. Bottom, left to right: classification of voxels for the defined lesion using the median value for perfusion; classification of voxels for the defined lesion using the median value for volume distribution of ^{18}F -FAZA; and multiparametric classification, combining perfusion and volume of tracer distribution.

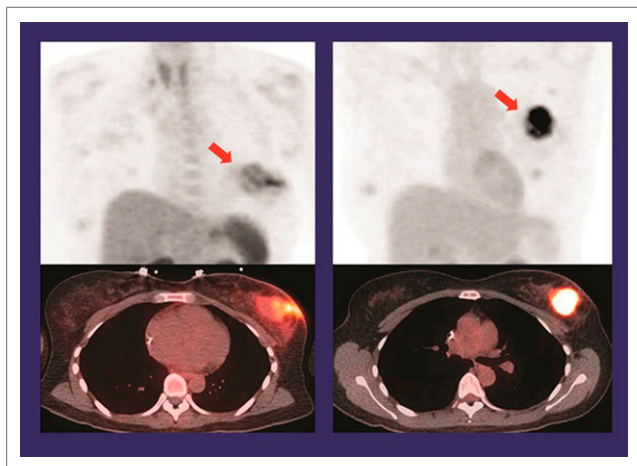


FIGURE 13. Comparison of ^{18}F -FPPRGD₂ (left) and ^{18}F -FDG (right) PET (top) and PET/CT (bottom) in a patient with breast cancer. $\text{SUV}_{\text{max}} = 6.1$ for ^{18}F -FPPRGD₂ and 19.6 for ^{18}F -FDG. Lack of spatial correlation between uptake of the 2 tracers helps confirm that each provides independent information.

with standard or intensive therapy, the researchers were able to confirm the value of interim PET in predicting response or nonresponse across treatment arms after 2 cycles of R-CHOP for NHL, as has been shown in smaller studies. Average times to treatment failure were 73 and 43 months, and overall survival rates at 3 years were 87% and 62%, for responders and for nonresponders, respectively.

Tumor hypoxia is an important topic for ongoing investigation, especially in radiation therapy, with a number of current approaches to hypoxia imaging, including the use of ^{18}F -fluoroazomycinaraboside (^{18}F -FAZA) PET. To gain insight into the relationship between perfusion and hypoxia, Iqbal et al. from the VU University Medical Center (Amsterdam, The Netherlands) looked at “Multiparametric evaluation of tumor hypoxia and perfusion using [^{15}O]H₂O and

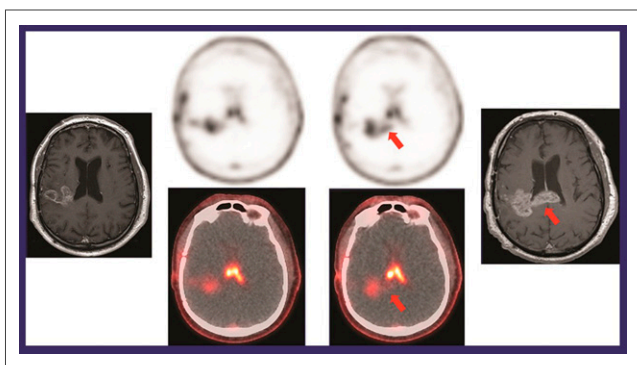


FIGURE 14. ^{18}F -FPPRGD₂ PET/CT in a patient with a glioma. Left: baseline brain MR. Middle block: PET (top) and PET/CT (bottom) images at baseline ($\text{SUV}_{\text{max}} = 3.3$) and after 1 wk of antiangiogenesis therapy ($\text{SUV}_{\text{max}} = 2.6$). Right: MR image after 4 weeks of antiangiogenesis therapy. This case indicated that the tracer could predict lesion response to avastin therapy at a very early phase and confirmed that ^{18}F -FPPRGD uptake in normal tissue was not affected by avastin therapy.

^{18}F -FAZA PET in NSCLC patients” [158]. Imaging hypoxia in tumors is challenging: when they are normoxic, this limits ^{18}F -FAZA retention. What is interesting is that as the tumor becomes more and more hypoxic, at first ^{18}F -FAZA is increased, but then becomes limited as perfusion becomes limited. This may result in false-negative ^{18}F -FAZA results, masking the presence of significant hypoxia. These investigators studied 8 patients with NSCLC who underwent dynamic [^{15}O]H₂O and ^{18}F -FAZA PET imaging with arterial sampling. Parametric analyses were performed to generate 3D images of both perfusion and volume of distribution of the tracer (Fig. 12). When these 2 parameters were correlated, the researchers found in some cases a positive association (6 lesions), in others a negative association (3 lesions), and in still others an intermediate association (4 lesions). These results suggest that spatial variation of ^{18}F -FAZA uptake is not necessarily inversely related to perfusion, so that for assessment of hypoxia using ^{18}F -FAZA PET, concomitant measurement of perfusion may be essential. Low ^{18}F -FAZA uptake does not guarantee normoxic conditions, and perfusion data are required to rule out flow-limited delivery.

Many different targets in cancer are the focus of ongoing research. Minamimoto et al. from Stanford University (CA) reported on “ ^{18}F -FPPRGD₂ PET as a surrogate marker of integrin $\alpha_v\beta_3$ expression before and after anti-angiogenesis treatment” [629]. The researchers looked at 31 patients (17 glioblastoma, 8 breast, 4 NSCLC, 1 ovarian, 1 cervical cancer), analyzing the biodistribution of the agent across a variety of cancer lesions and normal tissues and comparing uptake of ^{18}F -FPPRGD₂ and ^{18}F -FDG. They also

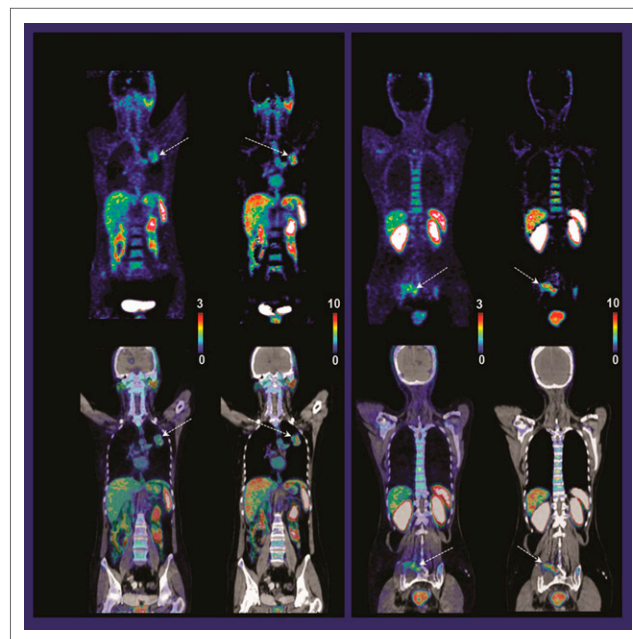


FIGURE 15. Dynamic ^{68}Ga -PRGD₂ whole-body parametric mapping. Patient with primary tumor in lung and metastasis in pelvis. Top: Static PET images at 1 h and parametric maps; arrows = primary tumor and metastasis. Bottom row: Corresponding PET/CT images.

looked at these imaging values before and after antiangiogenesis therapy. Evaluating PET imaging in a patient with breast cancer, they found no correlation between ^{18}F -FPPRGD2 and ^{18}F -FDG PET, indicating that the information provided by each tracer is independent (Fig. 13). The arginine-glycine-aspartic acid (RGD) agent images the integrin expression, and the FDG agent images metabolism. The investigators looked at ^{18}F -FPPRGD2 uptake on PET/CT with corresponding MR imaging in glioma patients before and after therapy with avastin. Figure 14 shows PET/CT imaging in such a patient, including baseline and post-antiangiogenic therapy MR imaging. Although the RGD imaging was able to assess change in integrin expression, this is a patient in whom the therapy was not ultimately effective. This imaging approach has the potential to guide early selection of alternative therapies for patients in whom treatments like avastin therapy are not working.

Guo et al. from the Massachusetts General Hospital/Harvard Medical School (Boston), the Peking Union Medical College Hospital (Beijing, China), and the National Institute

of Biomedical Imaging and Bioengineering (Bethesda, MD) reported on “Whole-body parametric imaging of lung cancer patients with ^{68}Ga -PRGD2” [122]. In addition to studying the pharmacokinetics of this tracer, the group performed dynamic PET scans with a shuttling imaging bed covering 4 bed positions in each time frame. They were able not only to look at static SUV images of tumors, reflecting integrin expression, but to produce parametric maps with information on binding potential and other data (Fig. 15). This approach has the potential to provide enhanced tumor-to-background contrast and better quantitation of uptake across multiple metastatic sites in a single patient. They were able to calculate volume of distribution and binding potential across primary and metastatic sites, including bone and nodal metastases. Whole-body kinetic analyses and parametric maps showed promise for quantitatively assessing whole-body-range integrin expression and may potentially help guide drug therapy dosing.

This highlights lecture will be continued in Newsline in the December issue of JNM.